Journal of Hazardous Materials 201–202 (2012) 23–32

Contents lists available at SciVerse ScienceDirect

Journal of Hazardous Materials

journal homepage: www.elsevier.com/locate/jhazmat

Mesoporous aluminosilica monoliths for the adsorptive removal of small organic pollutants

Sherif A. El-Safty[a,b,c,*], Ahmed Shahat[a], Mohamed Ismael[a]

[a] National Institute for Materials Science (NIMS), 1-2-1 Sengen, Tsukuba-shi, Ibaraki-ken 305-0047, Japan
[b] Department of Chemistry, Faculty of Science, Tanta University, Tanta, Egypt
[c] Graduate School for Advanced Science and Engineering, Waseda University, 3-4-1 Okubo, Shinjuku-ku, Tokyo 169-8555, Japan

ARTICLE INFO

Article history:
Received 7 February 2011
Received in revised form 19 October 2011
Accepted 31 October 2011
Available online 7 November 2011

Keywords:
Mesoporous aluminosilica
Monoliths
Cubic structures, Organic pollutants
Nano-adsorbent
Anilines
Adsorption
Removal

ABSTRACT

Water treatment for the removal of organic or inorganic pollutants has become a serious global issue because of the increasing demand for public health awareness and environmental quality. The current paper, reports the applicability of mesoporous aluminosilica monoliths with three-dimensional structures and aluminum contents with $19 \leq Si/Al \geq 1$ as effective adsorbents of organic molecules from an aqueous solution. Mesocage cubic *Pm3n* aluminosilica monoliths were successfully fabricated using a simple, reproducible, and direct synthesis. The acidity of the monoliths significantly increased with increasing amounts of aluminum species in the silica pore framework walls. The batch adsorption of the organic pollutants onto (10 g/L) aluminosilica monoliths was performed in an aqueous solution at various temperatures. These adsorbents exhibit efficient removal of organic pollutants (e.g., aniline, p-chloroaniline, o-aminophenol, and p-nitroaniline) of up to 90% within a short period (in the order of minutes). In terms of proximity adsorption, the functional acid sites and the condensed and rigid monoliths with tunable periodic scaffolds of the cubic mesocages are useful in providing easy-to-use removal assays for organic compounds and reusable adsorbents without any mesostructural damage, even under chemical treatment for a number of repeated cycles.

1. Introduction

Water pollution results in serious health problems, particularly in third world countries. The considerable contamination of the aqueous environment by organic pollutants still requires the development of quick and simple methods for the removal, separation, and determination of these compounds [1,2]. A common problem in many industries is the disposal of large volumes of wastewater containing major classes of these organic compounds, which are carcinogenic and mutagenic, with high toxicological potentials. Among these discharged pollutants, aniline compounds are one of the most important organic intermediates that are widely used in the manufacture of conducting polymers, rubbers, drugs, dyes, and pesticides [2]. The potential use of aniline compounds resulted in their large-scale disposal into wastewater. For example, nitroaniline is a highly toxic agent to humans that is absorbed through the skin or through inhalation [3]. Exposure to this organic substance can result in a condition called methemoglobinemia, which is characterized by changes in the blood. Hemoglobin is specifically converted into methemoglobin. Such a conversion results in the impairment of blood cells, consequently reducing their capacity to transport oxygen [4].

Efficient techniques for the removal of these highly toxic compounds from water have drawn significant interest [5]. Among the possible techniques for water treatments, the adsorption process by solid adsorbents shows potential as one of the most attractive and efficient methods for the purification and separation of trace organic contaminants in wastewater treatment [5]. Various adsorbents, such as organic clay [6], silica gel [7], zeolites [8], montmorillonite [9], resins [10], polymers [11], activated carbons [12a], α-Al_2O_3 [12b], and iron powders [13], have been used for the removal of aniline compounds from wastewater. Although these solid materials are commonly used as efficient adsorbents for the removal of organic pollutants from contaminated water, particularly activated carbons, the development of new adsorbent materials that can enhance the adsorption capacity and affinity and of reproducible and reversible assays is still necessary [3,14,15].

Mesoporous molecular sieves have received increasing interest from the scientific community because of their unique properties [16–20]. Mesoporous materials have been identified as promising adsorbents for biochemical molecules, such as amino acids,

* Corresponding author at: National Institute for Materials Science (NIMS), 1-2-1 Sengen, Tsukuba-shi, Ibaraki-ken 305-0047, Japan and Graduate School for Advanced Science and Engineering, Waseda University, 3-4-1 Okubo, Shinjuku-ku, Tokyo 169-8555, Japan. Tel.: +81 298592135; fax: +81 298592025.
E-mail addresses: sherif.elsafty@nims.go.jp, sherif@aoni.waseda.jp (S.A. El-Safty).

0304-3894/$ – see front matter © 2011 Elsevier B.V. All rights reserved.
doi:10.1016/j.jhazmat.2011.10.088

peptides, and proteins [16]. For instance, mesoporous silica can also be used to remove some organic and inorganic pollutants from water [15,17,18]. Bibby and Mercier used cyclodextrin-functionalized mesoporous silicas as adsorbents for different water-soluble aromatic molecules, including p-nitrophenol and p-nitroalinine [19]. The open-framework nature and large pore size (2–50 nm) of mesoporous adsorbents are the key components for the fast adsorptivity and accessibility of the molecules to the binding sites [18,19]. Arumugam and Perumal reported that neutral alumina adsorbents could be used for developing a new purification process for pharmaceutical and chemical wastes, such as benzophenone, aniline, p-nitroaniline, and resorcinol [20]. Zeolites with different pore orientations and organizations have been used to remove p-nitroaniline molecules from an aqueous medium [21].

Recently, the increasingly stringent device requirements based on mesoporous materials for advanced applications, such as catalysis [22], sensing [23], molecular transport and separation [24], and multifunctional designs [25], have demanded modulated pore structures, functional surface chemistry, and the incorporation of heteroatoms, such as aluminum [22,26–32]. In this regard, the synthesis of aluminosilica monoliths with high acidity and structural integrity may result in the expansion of widespread applications [33–35]. The current research efforts focus on two critical issues: (1) the fabrication of three-dimensional (3D) cubic *Pm3n* nanoscale monolithic discs as membrane platforms and (2) the design of easy-to-use, portable, and reusable chemical adsorbents for the removal of up to 90% of organic pollutants within a short period (in the order of minutes) from an aqueous solution.

2. Experiments

2.1. Synthesis of cubic Pm3n aluminosilica monolithic adsorbents

The simple synthesis process for monolithic aluminosilica adsorbents was based on the direct templating of the microemulsion liquid crystalline phase of the Brij 56 surfactant. In this direct synthesis of cubic *Pm3n* aluminosilica monoliths, for example, at the Si/Al ratio of 9 (w/w) and at a Brij 56/tetramethylorthosilicate (TMOS) ratio of 0.5 (w/w), the precursor solution [1 g of Brij 56, 0.5 g dodecane, 2 g TMOS, 0.569 g $Al(NO_3)_3$, 2.5 g H_2O–HCl (at pH 1.3), and 10 g of ethanol] was stirred for 30 min to form a homogenous sol–gel solution. The resulting optical gel-like mixture was placed in a graduate ingot. The mixture subsequently acquired the shape and size of the cylindrical casting vessel. The monoliths were gently dried at room temperature for 2 h and then allowed to stand in a tightly closed ingot for 1 day to complete the drying process (Scheme 1).

To obtain monolithic samples with various aluminum contents at the Si/Al ratio of 19, 10, 4, 2.3, 1.5, and 1, the molar composition of $Al(NO_3)_3$ was varied from 0.7×10^{-3} mol to 13.6×10^{-3} mol (see Table S1, Supporting information). The organic moieties were removed by calcination at 550 °C under air for 5 h. The calcined cage cubic *Pm3n* monoliths clearly had stable and tough discs with 1.2 mm thickness and ~12 mm length. In turn, the transparency of the monoliths was lost by calcination [18,36]. In addition, Al/SBA-15 aluminosilica powder was synthesized using the conventional hydrothermal method (see Supplementary materials). Advanced characterization techniques, such as N_2 adsorption isotherms, X-ray diffraction (XRD), transmission electron microscopy (TEM) and three-dimensional TEM surfaces (3D TEM), energy dispersive X-ray microanalyzers (EDX), ^{27}Al magic-angle spinning nuclear magnetic spectroscopy (^{27}Al MAS NMR), and NH_3 temperature-programmed desorption (NH_3-TPD), were used for the determination of the structural, textural, and physicochemical properties of aluminosilica adsorbents (see Supplementary materials).

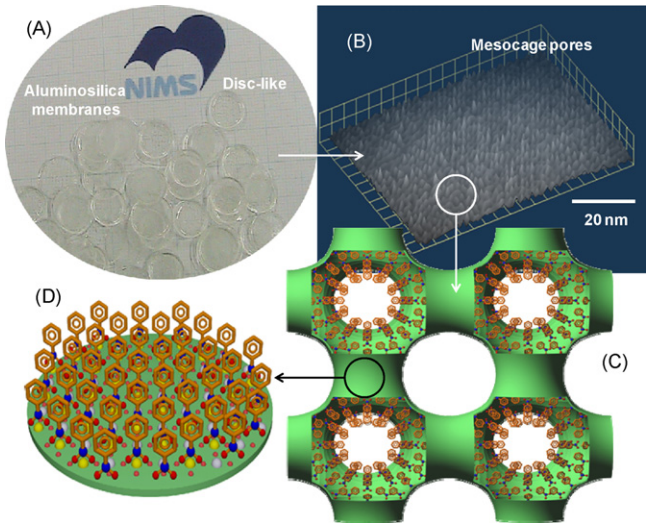

Scheme 1. Aluminosilica monoliths with a disc-like shape (A) and mesocage pores (B) as adsorbents (C) of organic compounds (**I–IV**) inside the mesocage cavity and onto pore surfaces of 3D cubic *Pm3n* structures (D). Note that 3D TEM image (B) was recorded with aluminosilica monoliths with a Si/Al ratio of 4.

2.2. Batch adsorption method of organic pollutants

The batch adsorption of the organic pollutants (**I**, **II**, **III,** and **IV**) onto (0.2 g) aluminosilica monoliths was performed in an aqueous solution at different temperatures (30–45 °C, ±0.1 °C range). The adsorption process was performed using a shaker thermostat, where the shaking rate was kept constant for all experiments. The initial concentration of adsorbates in the range of 5×10^{-3} mol/L to 8×10^{-4} mol/L was measured using a Shimadzu 3700 model solid-state ultraviolet–visible spectrophotometer at specific wavelengths of 287, 289, 289, and 262 nm for **I**, **II**, **III**, and **IV** molecules, respectively. The adsorption amount (q_e, mmol g^{-1}) of the molecules at the equilibrium step was determined according to the following equation:

$$q_e = \frac{C_o - C_e}{V} m \quad (1)$$

where V is the solution volume (L); m is the mass of monolithic adsorbents (g); and C_o and C_e are the initial and equilibrium adsorbate concentrations, respectively. The percentage uptake ($\%U$) of the adsorbate solutes at the adsorption equilibrium was calculated using the following equation:

$$\% U = \frac{C_o - C_e}{C_o} \times 100 \quad (2)$$

The fraction of the coverage mesocage adsorbent surfaces (f_c, g/m^2) occupied by the pollutant molecules was calculated according to the following equation:

$$f_c = \frac{M\beta}{S} \quad (3)$$

where M is the molecular area of pollutant molecules in the range of 63–70 Å^2 [17], S (m^2/g) is the surface area of the monolithic adsorbents, and β is the number of molecules adsorbed per unit area of mesocage adsorbents. However, β can be calculated as follows: $\beta = (q_e/S) \times N_A$, where N_A is Avogadro's number (6.02×10^{23} mol^{-1}).

The intraparticle diffusion of pollutants into mesocage adsorbents can be determined by plotting the fractional attainment of equilibrium $F_e = q_t/q_f$ against $t^{1/2}$ according to Fick's second law relationship [37]:

$$F_e \left(\frac{q_t}{q_f}\right) = \frac{6}{r\sqrt{Dt/\pi}} \quad (4)$$

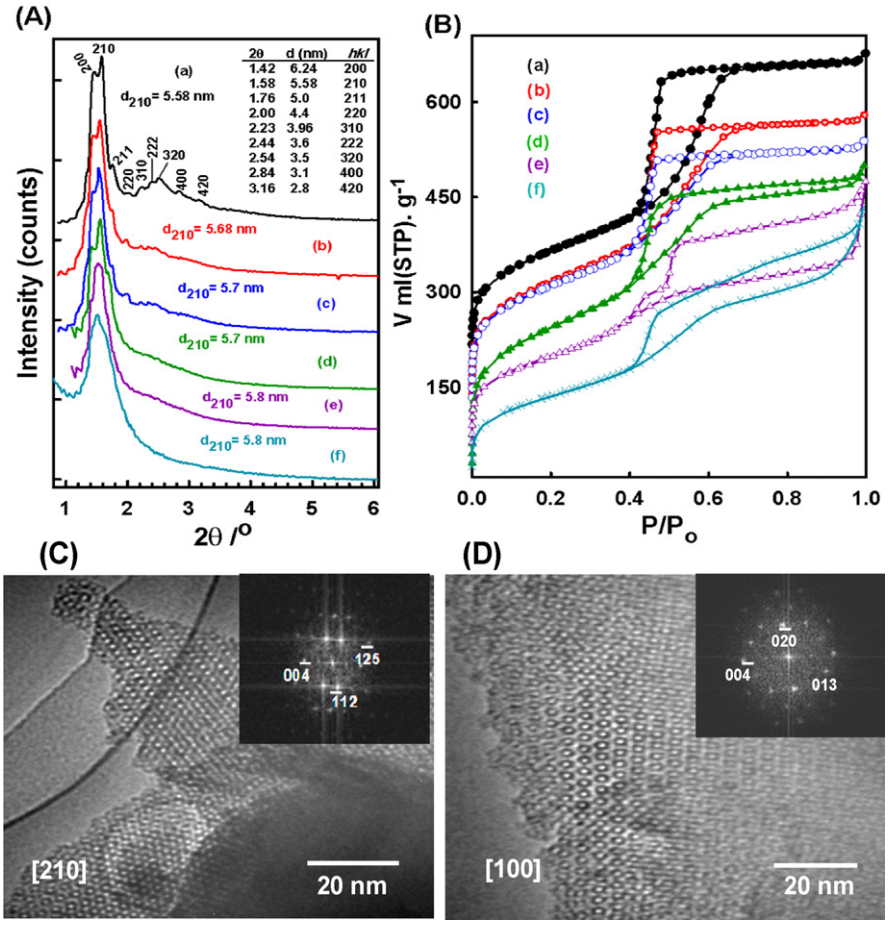

Fig. 1. XRD (A), N_2 isotherms (B), and HRTEM (C and D) patterns of cubic *Pm3n* aluminosilica monoliths with Si/Al ratios of 19 (a), 9 (b), 4 (c), 2.33 (d), 1.5 (e), and 1 (f). Note that the representative HRTEM micrographs and FTD (inserts) patterns (C and D) of calcined cubic *Pm3n* aluminosilica monoliths were recorded with Si/Al ratios of 9. The HRTEM and FTD patterns were recorded along the [2 1 0] (C) and [1 0 0] (D) zone axes, respectively.

where q_t/q_f is the ratio of the adsorbed quantity of the pollutant molecules at time (t) to the amount adsorbed at saturation time, r is the pore radius of mesocage adsorbents, π is a constant, and D is the intraparticle diffusion coefficient.

The thermodynamic equilibrium constant (K_c), which is dependent on the fractional attainment of equilibrium (F_e) of the adsorbed molecules, can be deduced from the following equation [37]:

$$K_c = \frac{q_f}{1 - q_f} \tag{5}$$

where q_f can be determined from the ratio of the number of molecules adsorbed at a given time (q_t) to that adsorbed at infinity (q_α) (i.e., $q_f = q_t/q_\alpha$).

The batch adsorption of organic pollutants (**I**, **II**, **III**, and **IV**) onto the aluminosilica monolith adsorbents was analyzed using Lagergren first-order kinetics, according to the following equation [17]:

$$\ln(q_e - q_t) = \ln q_e + k_t t \tag{6}$$

where k_t is the rate constant (per gram adsorbent, pga) of the first-order kinetics.

The adsorption characteristics of a solute onto the adsorbent can be studied through the Langmuir isotherm [17,37]:

$$\frac{C_e}{q_e} = \frac{1}{K_L q_m} + \left(\frac{1}{q_m}\right) C_e \tag{7}$$

where q_m (mmol g^{-1}) is the amount of adsorbate adsorbed to form a monolayer coverage, and K_L is the Langmuir adsorption equilibrium constant. From the plot of C_e/q_e against C_e, q_m, and K_L can be determined from the slope and the intercept.

3. Results and discussion

3.1. Textural and physicochemical properties of aluminosilica monolith adsorbents

The synthesis of aluminosilica monoliths with active acid sites, multidirectional (3D) pore connectivity, well-defined cage cavities, and disc-like shape is promising for easy-to-use adsorbents for organic molecules within a short period (within minutes). The 3D TEM micrographs (Scheme 1B) show that the uniform pore surfaces of the mesocage monoliths were decreased with high aluminum contents. The uniformity of the pore surface not only results in a facile accessibility of the organic molecules (Scheme 1C), but also increases the homogeneous transport of the molecules from the aqueous phase to the nano-adsorbent surfaces (Scheme 1D).

The 3D cage cubic *Pm3n* aluminosilica monoliths were successfully fabricated throughout the phase transformation mechanism [22b,36]. In the microemulsion phase domains, the addition of alkane with long alkyl chain lengths (dodecane) to the Brij 56/TMOS/aluminum salt mixture substantially affected the formation of 3D mesophase and the enlargement of pore sizes of the aluminosilica mesostructures [36]. In the current report, the solubilization of alkane into the hexagonal phase domains of Brij 56 resulted in the hexagonal *P6mm*-cubic *Pm3n* phase transition with shape- and size-controlled cage pores, as evidenced from the XRD

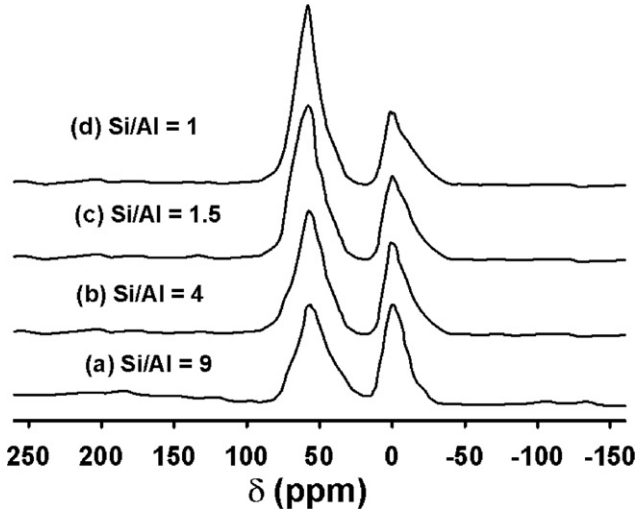

Fig. 2. ^{27}Al MAS NMR spectra of cage cubic *Pm3n* aluminosilica monoliths with Si/Al ratios of 9 (a), 4 (b), 1.5 (c), and 1.0 (d).

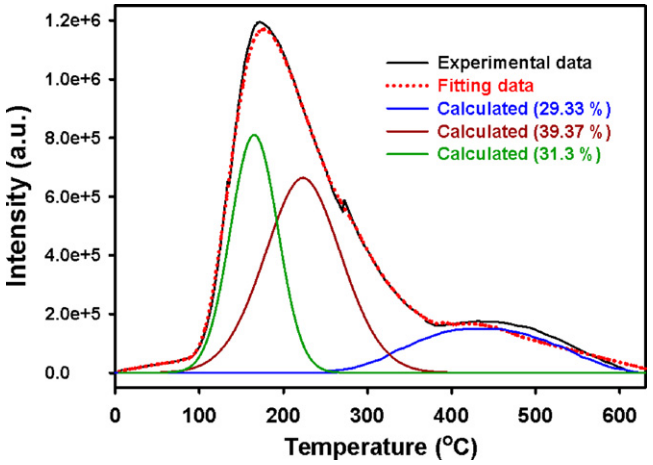

Fig. 3. NH_3-TPD spectra and a deconvolution of each peak of cage cubic *Pm3n* aluminosilica monoliths fabricated with Si/Al ratio of 9.

patterns (Fig. 1A). The XRD patterns (Fig. 1A) of the monoliths with low aluminum content (Si/Al < 4) show well-resolved diffraction peaks that tentatively result in the assignment of ordered cubic *Pm3n* geometries (Fig. 1Aa–c). The resulting XRD reflection peaks (Fig. 1Ad–f) indicate that the aluminum contents resulted in a decrease in the structural ordering of monoliths. However, the addition of a large amount of aqueous aluminum salt to the synthesis composition domains increases the polar volume fractions, thus increasing the unit-cell constants of the cubic structures [38].

The N_2 adsorption isotherms (Fig. 1B) of aluminosilica monoliths showed an H2-type hysteresis loop and well-defined steepness of isotherms, indicating that uniform cage-like pore structures were characteristic of the cubic *Pm3n* aluminosilica monoliths [39]. With hexagonal Al/SBA-15 adsorbents, the isotherms showed a pronounced H1-type hysteresis loop, indicating the formation of open cylindrical pore size of ~6.0 nm [39]. Generally, the adsorption branches significantly shifted toward a lower relative pressure (P/P_o) with increasing aluminum contents. Based on the N_2 isothermal results, the cage aluminosilica monoliths and cylindrical powders (Al/SBA-15) were observed to have the appreciable textural parameters of specific surface area (S_{BET}), mesopore volume, and tunable pore diameters. The decrease in these textural parameters was observed because of the structural ordering degradation with high aluminum contents of monoliths (see Table 1).

The TEM images (Fig. 1C and D) showed that the 3D mesoscopic qualities of the aluminosilica monoliths still retained their long-range structural ordering over a large area, even for samples with Si/Al ratios as high as four. The overall TEM lattice images and corresponding Fourier transform diffractogram (FTD) patterns (inserts) recorded along the [2 1 0] and [1 0 0] indices indicated the formation of cubic *Pm3n* structures. The FTD images show specific lattice fringes along the zone axes of cubic *Pm3n* lattice symmetries. With low silica contents ($1.5 \leq Si/Al \leq 1$), representative TEM images (see Fig. S1) revealed a short-range ordering or even worm-like mesopore channels interconnecting in large-sized domains.

The coordination state of the aluminum species was investigated using ^{27}Al NMR (see Fig. 2). In all the aluminosilica samples ($19 \leq Si/Al \leq 1$), two ^{27}Al peaks centered at the chemical shift of −1 and 58 ppm, indicating the existence of octahedral (Al^{VI}, AlO_6, extra framework) and tetrahedral (Al^{IV}, AlO_4, framework) aluminum sites, respectively. Tetrahedrally coordinated aluminum sites were significantly increased with increasing aluminum contents in the mesocage monoliths, as evidenced by the increase in the Al^{IV}/Al^{VI} ratio from 1.08 to 2.33 (see Table S1). The coordination and location of aluminum sites in the frameworks play a key role in the generation of the surface acidity of aluminosilica monoliths, as evidenced by the NH_3 temperature-programmed desorption (NH_3-TPD) profiles.

The TPD profiles show two main peaks of NH_3 desorption at approximately 200 °C and a small, broad intensity peak in the range of 400–500 °C (Fig. 3). These peaks indicated that two types of acid sites were characterized by aluminosilica monoliths with all Si/Al ratios, as evidenced by the deconvolution analysis of the desorption curve (Fig. 3). To quantitatively determine the amount and strength of acid sites of mesoporous aluminosilica, the peaks at approximately 200 °C and 450 °C were deconvoluted using the Gaussian function, with temperature as the variant. The components of the peaks at approximately 200 °C and 450 °C were 60.63% and 39.33%, respectively. These component ratios indicated that ammonia was desorbed from the weak "Lewis" and mildly strong "Bronsted" acid sites of the OH-groups of aluminosilica adsorbents. Furthermore, the number of acid sites increased with the amount of aluminum (see Table S1), which is in agreement with recent reports [40]. The enhancement of surface acidity might result in a strong interaction between the surface functional groups of the adsorbents and the adsorbates.

3.2. Batch contact-time adsorption experiments

The removal of the aluminosilica nano-adsorbent with different organic pollutants (**I**–**IV**) was conducted through batch contact-time experiments in an aqueous solution. The adsorbed amount as a function of the exposure time of the organic pollutants to the monoliths was studied using UV–vis spectroscopy.

Fig. 4A shows the time-rate dependence of the adsorption amount of molecule solutes (**I**, **II**, **III**, and **IV**) using mesocage monolithic adsorbents at specific conditions (i.e., 40 °C, adsorbent dose of 10 g/L, adsorbate concentration of 1.6×10^{-3} mol/L, and constant shaking rate). Fig. 4B reveals the adsorbed amount as a function of the initial concentration of adsorbates (C_o, mol/L) in the range of 5×10^{-3} mol/L to 8×10^{-4} mol/L. Results reveal the increase in the adsorption amount of monolith adsorbents with increasing initial concentration. Fig. S2 shows the effect of the concentration range on the adsorbed concentration of adsorbates (**I**–**IV**). A linear graph in the range of 8×10^{-4} mol/L to 1.6×10^{-3} mol/L of the adsorbate concentration, with a correlation coefficient range of 0.98–0.99, was characteristic of the adsorption curves for all adsorbates. However, the saturation effects resulted in a nonlinear

Table 1
Synthesis conditions, as well as structural and textural parameters of cage cubic *Pm3n* aluminosilica monolith adsorbents fabricated using the microemulsion phases of Brij 56 as soft templates and with a wide range of Si/Al ratios (w/w) in a preparation gel. Unit cell parameter (a), BET surface area (S_{BET}), NLDFT mesopore size (R), and total pore volume (V_p).

Monoliths with Si/Al ratios (w/w)	Synthesis conditions				EDX analysis	Structure parameters			
	$10^2 \times T^{[a]}$ (mol)	$(10^3) \times Al(NO_3)_3$ (mol)	Brij 56/TMOS (w/w)	Si:Al	Si:Al (±0.01)	$a^{[b]}$ (nm)	$S_{(BET)}$ (m^2/g)	R (nm)	$V_{(mesopore)}$ (cm^3/g)
19	1.31	0.7	0.5	1:0.053	1:0.0536	12.5	700	4.7	0.73
9	1.31	1.5	0. 5	1:0.11	1:0.111	12.7	780	4.7	0.81
4	1.31	3.4	0. 5	1:0.25	1:0.253	12.7	560	4.6	0.74
2.3	1.31	5.8	0.5	1:0.43	1:0.433	12.7	475	4.4	0.76
1.5	1.31	9.1	0. 5	1:0.66	1:0.673	13.0	440	4.2	0.64
1.0	1.31	13.6	0.5	1:1	1:1.02	13.0	430	4.4	0.53
9[a]	0.96	1.06	0.5	1:0.11	1:0.111	9.9	740	6.0	0.75

$T^{[a]}$, TMOS; $a^{[b]}$, and unit cell parameter ($a_{Pm3n} = d_{210}\sqrt{5}$, and $a_{P6mm} = 2d_{100}\sqrt{3}$).
[a] Hexagonal Al/SBA-15 adsorbents fabricated using Pluronic P123 and TEOS as template and silicon sources, respectively.

correlation at the inflection point with high concentrations ($\geq 1.6 \times 10^{-3}$ mol/L). The nonlinear adsorption curves indicated that the low concentrations of the adsorbates (**I**–**IV**) can be removed from aqueous water in a one-step treatment. Fig. 4C shows the temperature-dependent kinetic response of the *p*-Cl–Ar–NH_2 (**III**) adsorption. Results indicated that the increase in the temperature resulted in the increased activation energy of the adsorbates in the aqueous phase and consequently enhanced the adsorption amounts.

The relative adsorption affinity of the mesocage adsorbent for organic pollutants was decreased in the order of **I** < **II** < **III** < **IV**. Fig. 4D shows the fractional attainment of equilibrium F_e against $t^{1/2}$ of the monoliths. Evidently, Fig. 4B can be classified into three portions. First, the linear portion reflects the instantaneous adsorption stage. During this step, the monolithic particles of the adsorbents are considered to be surrounded by a boundary layer of fluid film, through which the adsorbate solute must diffuse prior to external adsorption on the adsorbent surfaces. The second part is the curve portion that signifies the intraparticle diffusion step, and the third portion is the final equilibrium stage. However, the intraparticle diffusion coefficient, D, is calculated from the slope of the second portion of Fig. 4B (Table 2) [17]. The plateau in Fig. 4D provides evidence that intraparticle diffusion might control the mass transport of the pollutant molecules from the aqueous phase to the aluminosilica monolith pores. However, one of the main features of aluminosilica monolith frameworks is the existence of micropores (4–5 Å) interconnecting the 3D ordered mesopores, which might make such a framework more suitable for

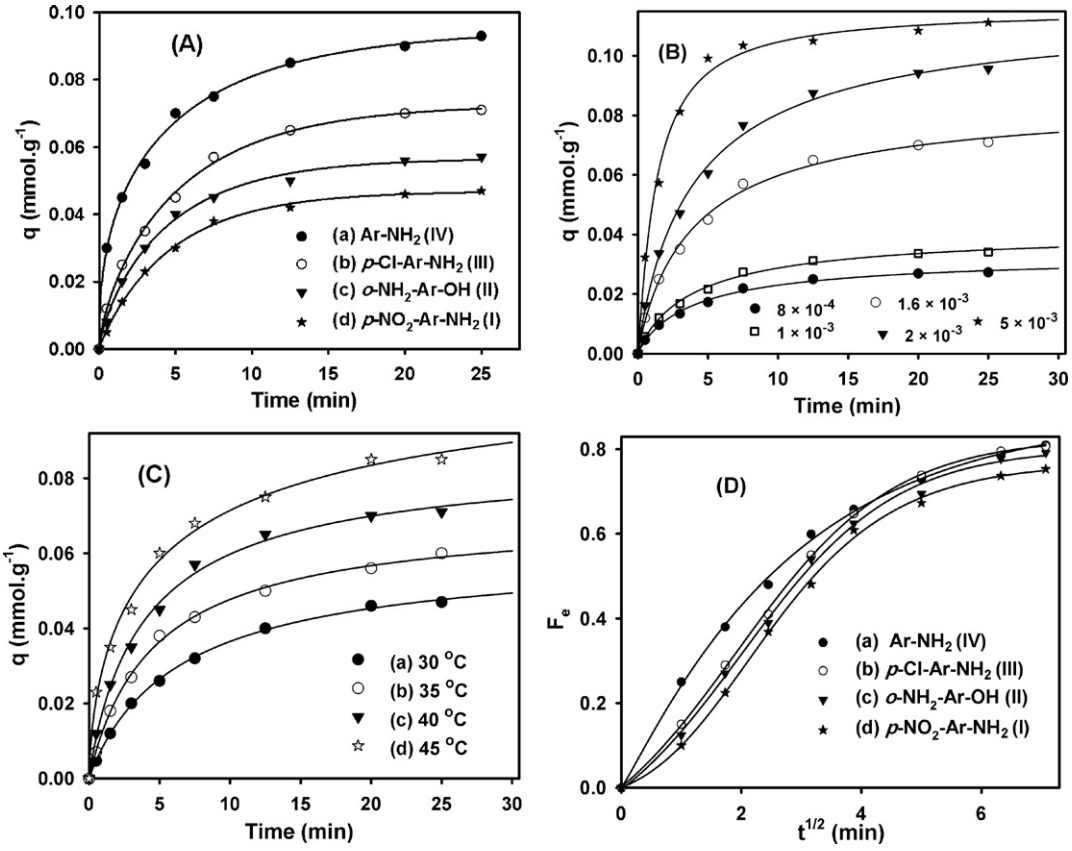

Fig. 4. Time–rate dependence of the adsorption amount of organic pollutants [1.6×10^{-3} M] (**I**, **II**, **III** and **IV**) (A). Effect of both concentration (B) and temperature (°C) on the time–rate dependence curve of the adsorption assay of *p*-Cl–Ar–NH_2 (**III**). Fractional attainment of the equilibrium of the adsorption assays (D) of [1.6×10^{-3} M] adsorbate molecules (**I**, **II**, **III**, and **IV**) onto [10 g/L] cage aluminosilicate-based adsorbents with a Si/Al ratio of 1.5 at 40 °C.

Table 2
Effect of the cage aluminosilica-based adsorbents [10 g/L] with different Si/Al ratios on the adsorption performance of [1.6×10^{-3} M] **I**, **II**, **III**, and **IV** pollutants at 40 °C.

Adsorbent	Adsorption properties											
Si/Al	Ar–NH_2 (IV)			*p*-Cl–Ar–NH_2 (III)			*o*-NH_2–Ar–OH (II)			*p*-NO_2–Ar–NH_2 (I)		
	$f_c \times 10^4$ (g/m^2)	$10^{17} \times D$ (cm^2/min)	q_m (mmol L^{-1})	$f_c \times 10^4$ (g/m^2)	$10^{17} \times D$ (cm^2/min)	q_m (mmol L^{-1})	$f_c \times 10^4$ (g/m^2)	$10^{17} \times D$ (cm^2/min)	q_m (mmol L^{-1})	$f_c \times 10^4$ (g/m^2)	$10^{17} \times D$ (cm^2/min)	q_m (mmol L^{-1})
19	2.5	2.05	0.12	1.88	1.44	0.08	1.35	0.73	0.07	0.97	0.27	0.05
9	3.3	3.18	0.17	2.66	3.38	0.10	2.15	2.02	0.08	1.51	0.87	0.07
4	5.8	4.54	0.20	4.72	5.52	0.16	3.71	4.56	0.09	3.04	2.32	0.08
1.5	11.4	9.36	0.14	8.76	6.26	0.13	7.72	6.48	0.12	6.41	4.54	0.11
1.0	14.8	14.79	0.34	11.7	16.98	0.26	10.6	9.68	0.21	9.28	8.49	0.19
9[a]	3.15	3.92	0.22	2.56	4.04	0.15	2.02	2.43	0.11	1.43	1.08	0.06

[a] The Al/SBA-15 adsorbents used for the removal of organic pollutants at the same experimental adsorption conditions.

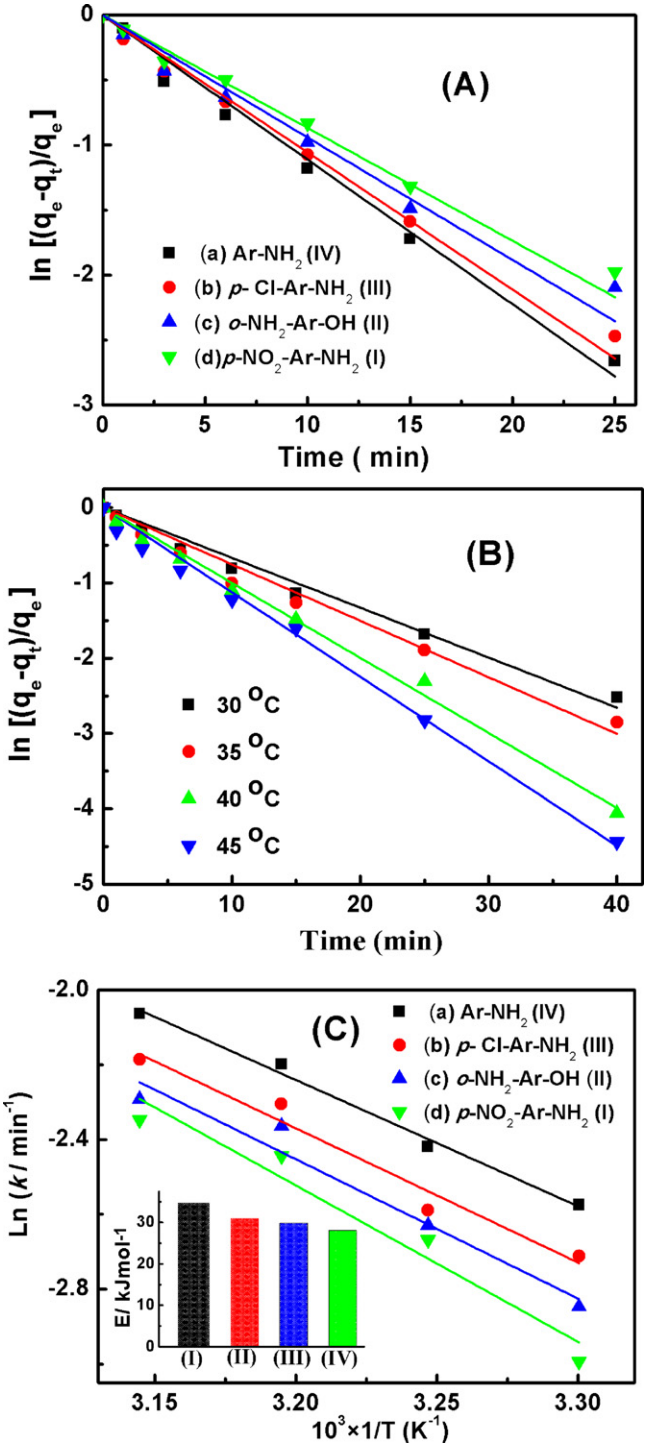

Fig. 5. Integrated first-order rate equation of the adsorption of the organic pollutants [1.6×10^{-3} M] (**I**, **II**, **III**, and **IV**) at 40 °C (A). (B) Effect of temperature on the adsorption rate of organic pollutant [1.6×10^{-3} M] (**III**). (C) Arrhenius plot of the adsorption of the organic pollutants [1.6×10^{-3} M] (**I**, **II**, **III**, and **IV**) onto [10 g/L] mesocage aluminosilica monoliths with a Si/Al ratio of 1.5.

the adsorption of these organic pollutants. These interconnecting pores facilitate the diffusion inside the entire micropore structure volume (V_m = 0.03–0.05 cm^3/g) [22,23,41] (see Fig. S4). These ordered monoliths with micro, meso, and macropore sizes are suitable for the adsorption of either small or bulk molecules [24].

High mass transport, homogenous intraparticle diffusion (D), and coverage surfaces (f_c) were significantly affected by the active functional acid sites (see Table 2). The calculated (f_c) and (D) values

Table 3
Illustration of the kinetic and thermodynamic parameters of the adsorption of [1.6×10^{-3} M] organic pollutants (**I**, **II**, **III**, and **IV**) into aluminosilica monolith adsorbents [10 g/L] with a Si/Al ratio of 1.5.

Adsorbate	T (°C)	k_t (min^{-1})	K_c	Kinetic parameters				Thermodynamic parameters		
				E_a (kJ mol^{-1})	$\Delta H^{\#}$ (kJ mol^{-1})	$\Delta S^{\#}$ (kJ mol^{-1})^1	$\Delta G^{\#}$ (kJ mol^{-1})	ΔG (kJ mol^{-1})	ΔH (kJ mol^{-1})	ΔS (J K^{-1} mol^{-1})
Ar–NH_2 (IV)	30	0.076	3.70	28.09	25.51	−182.27	82.11	−3.30	16.04	63.90
	35	0.089	4.18					−3.66		
	40	0.111	4.63					−3.98		
	45	0.127	4.99					−4.25		
p-Cl–Ar–NH_2 (III)	30	0.066	2.97	29.85	27.27	−177.73	82.46	−2.73	22.32	82.78
	35	0.075	3.49					−3.19		
	40	0.010	4.02					−3.62		
	45	0.112	4.50					−3.98		
o-NH_2–Ar–OH (II)	30	0.058	2.44	30.98	28.40	174.81	82.68	−2.25	18.44	68.51
	35	0.072	2.92					−2.74		
	40	0.094	3.19					−3.03		
	45	0.101	3.48					−3.29		
p-NO_2–Ar–NH_2 (I)	30	0.050	2.34	34.75	32.17	−163.32	83.00	−2.14	15.43	58.16
	35	0.069	2.66					−2.51		
	40	0.087	2.90					−2.77		
	45	0.096	3.13					−3.02		

of the ordered nanoscale adsorbents effectively increased with the high loading of aluminum contents [22b,30]. Although the monoliths with low Si/Al ratios show a distortion in the pore ordering and a decrease in the surface area and pore volumes (see Table 1), the enhancement of both f_c and D of the monolithic adsorbents was achieved (Table 2). Furthermore, the f_c and D parameters of the monolithic adsorbents were decreased in the order of **I** < **II** < **III** < **IV**. Based on this adsorption behavior, the lower adsorption effectiveness of these organic pollutants was clearly consistent with the higher basicity (i.e., higher pK_a) of these adsorbates, except with *o*-NH_2–Ar–OH (II). However, the pK_a values are 4.6, 3.97, 9.7, and 1.01 for **IV**, **III**, **II**, and **I** molecules, respectively. The finding trends, in general, are not in accordance with well-known adsorption behavior, in which stronger basic properties of aniline compounds (higher pK_a) result in a higher adsorption value. The noncorrelation adsorption behavior of *o*-NH_2–Ar–OH (II) with its pK_a value may be attributed to the high interaction affinity through the NH_2- and OH-groups of the adsorbate (II) molecule with the OH-groups of the solid adsorbents.

The kinetic and thermodynamic studies show further evidence of the adsorption behavior of these organic pollutants (Fig. 5 and Fig. S3). Fig. 5A and B show that the first-order kinetic equation best describes the data on molecule adsorption on monolith adsorbents. The values of the rate constant, k_t (pga), of molecule (**I**, **II**, **III**, and **IV)** adsorption were determined from the slope of the linear first-order kinetic equation. The kinetic studies exhibited that the k_t value decreases in the following sequence: **VI** > **III** > **II** > **I** (see Table 3), which represents the same sequence of the adsorption amounts and the f_c and D parameters of these adsorbates (Table 2 and Fig. 4A). Fig. 5B shows the increase of k_t with increasing temperature, indicating that k_t is only temperature dependent.

The activation energy, E of molecule (**I**, **II**, **III**, and **IV)** adsorption was deduced from an Arrhenius plot (Fig. 5C). Other activation parameters of the free energy of activation, $\Delta G^{\#}$, the enthalpy of activation, $\Delta H^{\#}$, and the entropy of activation, $\Delta S^{\#}$, were calculated from Eyring's equation and are listed in Table 3 (see Fig. S3). Results showed that the lower E value with higher k_t value is in agreement with the sequence of the adsorption affinity of the adsorbates in the monoliths. The values of the activation parameters (Table 3) are almost consistent with those found in other diffusion studies through the interior particle pores of a resin, reflecting the ease of diffusion of organic pollutants (**I**, **II**, **III**, and **IV**) through the interior micro, meso, and macroporous monoliths.

The plot of $\ln K_c$ vs. $1 = T$ (Fig. S3) gives the numerical values of ΔH of the adsorption of organic pollutants. ΔG and ΔS are calculated and presented in Table 3. The thermodynamic equilibrium constant, K_c, increased with temperature for all adsorption assays, whereas the absolute value of ΔG increases with decreasing temperature. This result indicates that adsorption is spontaneous and more favorable at high temperature, which confirmed an endothermic adsorption process. In addition, the ΔS value increases in this sequence: **IV** > **III** > **II** > **I**, contributing to a greater value of K_c and greater stability of thermodynamic adsorption.

The Langmuir isotherm is the simplest theoretical model for monolayer adsorption. Fig. 5A shows the adsorption isotherms of pollutant compounds, **I**–**IV**. The results (Fig. 6A) indicate the formation of a monolayer of pollutants on the nano-adsorbent monoliths. From the linear plot of the Langmuir isotherm (Fig. 6B, inserts), the monolayer adsorption capacity, q_m, and the Langumir coverage constant, K_L, were obtained. The q_m and K_L values were decreased in the order of **I** < **II** < **III** < **IV**. This tendency is consistent with the adsorption behavior of these compounds.

Fig. 7A shows that the percentage uptake (%U) of organic pollutants was effectively appended to the loading amount of the active function sites of the aluminum species into the adsorbents. The adsorption uptake depends on the amount of surface functional groups. All Lewis acid sites might transform into Bronsted acid sites because of the adsorption of organic molecules onto the aluminosilica monoliths in aqueous solutions [40]. The tendency of organic molecules to coordinate with Lewis acid sites is minimal. The number of Bronsted acid sites for aluminosilica monolith adsorbents is the key factors for the enhanced adsorption uptake with high Al contents. The adsorption amount of adsorbate molecules on the monolithic adsorbents also depends on the extent of the aluminum surface chemistry of the cage aluminosilica structures (Fig. 7A). However, the functional aluminum active sites of four- or six-coordinate species contribute to adsorbate molecule binding. Such a synergistic interaction did not show significant alteration of the chemical properties of the active aluminum species, as evidenced by the ^{27}Al NMR spectra recorded after adsorption assays (data not shown). The results (see Table S1) show that the increase in Al^{IV}/Al^{VI} ratios results in an enhanced adsorption amount of the pollutants. This finding indicates that the organic molecules might readily be adsorbed onto monoliths that show highly tetrahedral (Al^{IV}, AlO_4^-, framework) aluminum sites.

Furthermore, the mesostructural geometries and 3D dimensions of the aluminosilica adsorbents have significant effects on the overall adsorption uptake of organic molecules (see the relative

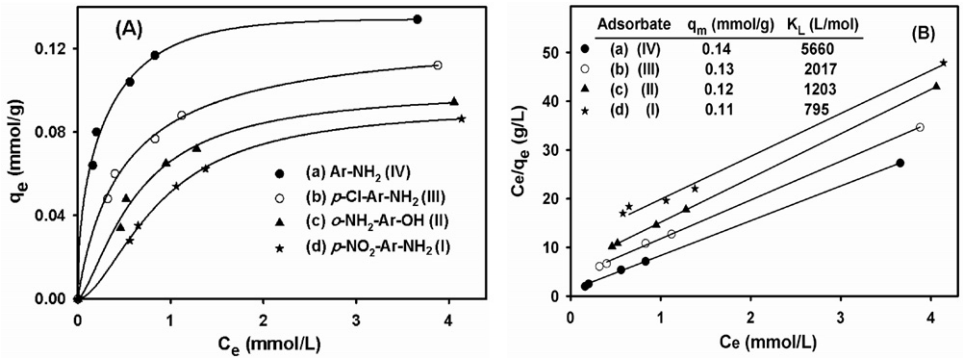

Fig. 6. The Langmuir adsorption isotherms (A) and the linear form of the Langmuir plot (B) of (**I**, **II**, **III**, and **IV**) onto [10 g/L] aluminosilica monolith adsorbents with a Si/Al ratio of 1.5 at 40 °C.

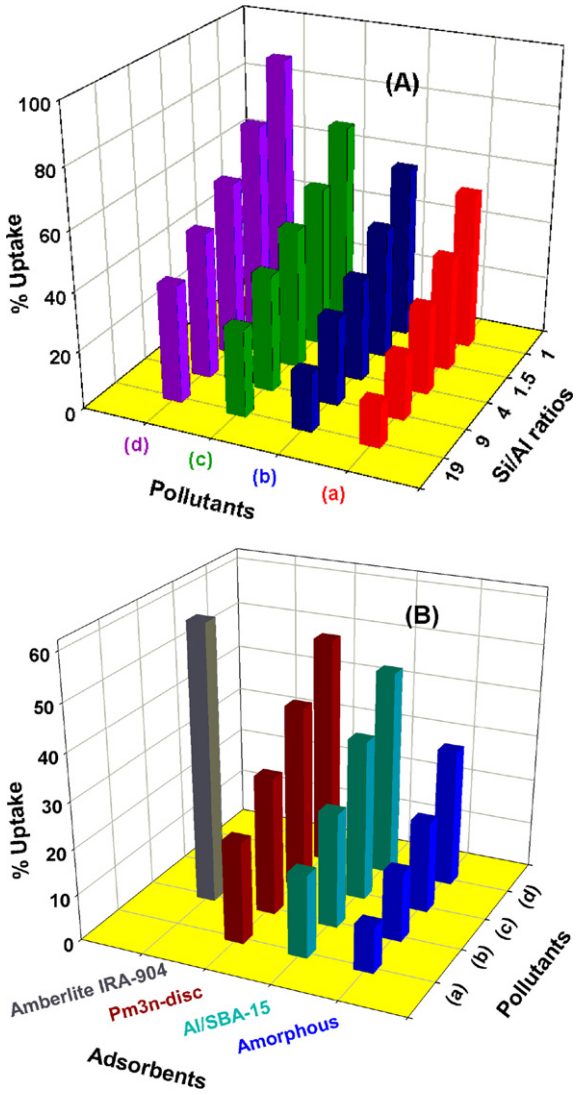

Fig. 7. Representative organic compounds uptake (A and B) of **I** (a), **II** (b), **III** (c), and **IV** (d) onto [10 g/L] cubic cage *Pm3n* aluminosilica adsorbents (monoliths) fabricated with different Si/Al ratios (A). To investigate the effect of ordered mesoporous monoliths, the uptake of **I** (a), **II** (b), **III** (c), and **IV** (d) onto [10 g/L] ordered powder Al/SBA-15 and amorphous aluminosilicas commercially supplied with a Si/Al ratio of 9 was studied (B). The uptake of **II** (b) was also studied onto [10 g/L] commercially supplied Amberlite IRA-904 anion exchange resin in chloride form (B). Batch contact-time experiments were conducted at 40 °C, equilibrium time, shaking rate, and at an adsorbate concentration (1.6×10^{-3} M).

adsorption uptake of the amorphous and ordered aluminosilicas at a Si/Al ratio of 9, Fig. 7B). The results (Fig. 7B) revealed that the ordered pore geometry had higher adsorption uptake of pollutants than the amorphous aluminosilica samples, indicating that the textural surface parameters (S_{BET}, as well as pore volumes and orders) and pore organizations significantly affected adsorption functionality in terms of intraparticle diffusion and binding coverage surfaces of pollutants onto the adsorbent monoliths (Fig. 7B).

To demonstrate the adsorption applicability of aluminosilica monolith adsorbents, adsorption experiments of the organic molecules using Amberlite IRA-904 anion exchange resin in chloride and mesoporous aluminosilicas (Al/SBA-15, powder forms) with a Si/Al ratio of 9 were conducted. However, although the monoliths had smaller pore sizes (~4.7 nm) than the Al/SBA-15 powder materials (Table 1), the former showed a higher adsorption amount (q), coverage surfaces (f_c), and percentage uptake ($\%U$) for all adsorbate molecules (Fig. 7B) [42]. In turn, the good distribution of the solute onto the powder aluminosilicas compared with monoliths made the diffusive mass transport into a small particle size, such as powder Al/SBA-15 materials, sufficiently rapid compared with the monoliths during the removal of all adsorbate samples (Table 2). The relatively high absorptivity of the monolith compared with Al/SBA-15 powder might be attributed to the larger particle size of micro-, meso-, and macro-porous monoliths compared with that of SBA-15 materials [42].

The adsorption uptake (%U) of molecule (**II**) using hierarchical monoliths was also compared with commercial and mature resin (Amberlite IRA-904) (Fig. 7B). Results indicated that both monoliths and Amberlite resin may act as effective adsorbents in terms of the overall uptake of adsorbates. Indeed, the monoliths are of interest because they offer easy-to-use removal assays and portable adsorbents compared with powder Al/SBA-15 or Amberlite IRA-904 materials, which require an intensive design during the adsorption and assessment monitoring of organic pollutants.

3.3. Adsorption/removal mechanism

Among these removal systems, the possible interactions between the adsorbate pollutants and aluminosilica monoliths are considered the driving forces for the molecular adsorption of pollutants. The adsorption sequence of these pollutants is correlated to the acid–base characteristic of the solute molecules and the loading content of aluminum into the pore surfaces. The substitution nature and relative position in the aromatic ring of molecule (**IV**) are significantly affected by the acid–base characters of the molecules based on the effect on the NH_2 bond strength. However, the coexistence of Ar–NH_2 compounds (**I**–**IV**) in an aqueous medium during adsorption can allow hydrogen bond-forming interactions with H_2O molecules (solvation). The effect of H_2O-pollutant

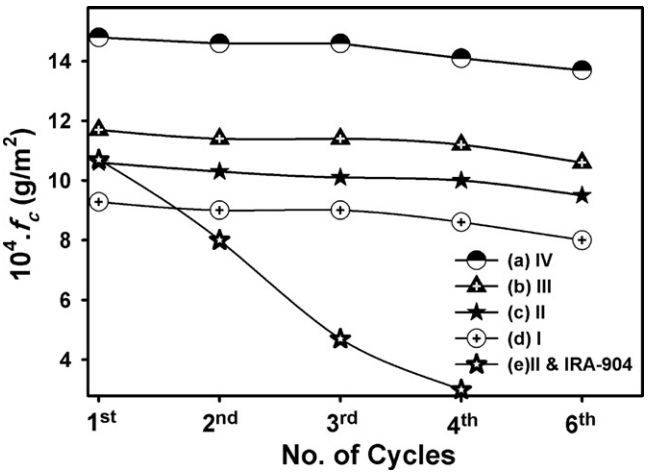

Fig. 8. Reusability study of up to six times for the removal assay of [1.6×10^{-3} M] **I** (a), **II** (b), **III** (c), and **IV** (d) onto [10 g/L] cage aluminosilicate adsorbents fabricated with a Si/Al ratio of 1. The reusability of o-aminophenol (*o*-NH_2–Ar–OH) (c,II) was also studied onto commercially supplied Amberlite IRA-904 anion exchange resin in chloride form at 40 °C.

molecular interactions increases with substituted Ar–NH_2 pollutants in the order of Cl < OH < NO_2 [43,44]. The strong interactions thereby render the mobility of these molecules on cage aluminosilica adsorbents less facile [43].

On the other hand, the insertion of aluminum into the solid mesocage monoliths resulted in the development of active acid sites at the internal mesopore surfaces of the adsorbents [23,27,28]. These natural surfaces of acid sites strongly induced both H-bonding and dispersive interactions with pollutant molecules. The adsorption behavior of pollutant molecules **I–IV** on mesocage aluminosilica is qualitatively considered according to the solvation affinities of **I–IV** molecules within the aqueous medium during the adsorption process, as previously reported on the adsorption onto other metal oxide surfaces, such as TiO_2 and Fe_2O_3 [44]. Generally, the current findings indicate that aluminosilica monoliths can act as effective adsorbents of the pollutant molecules from aqueous solutions.

3.4. Applicability of the adsorbents in recycling systems

The reusability of the adsorbent monoliths is of particular interest in developing recyclable adsorption systems. After a complete adsorption process, the mesocage solid monoliths were collected and repeatedly washed with an acidic aqueous solution [HCl = 1×10^{-3} M] and then dried at 200 °C for 12 h under air to remove the remaining molecular adsorbates. This feature enables more effective management by concentrating the collected pollutants, thereby reducing the volume of materials to be controlled. Measurements of the textural properties of the regenerated monoliths reveal that the specific surface area and mesopore volumes were slightly decreased (approximately 2–5% from the original data shown in Table 1). However, the pore shape and size were unchanged. Reused adsorbents are still effective for the adsorption of organic adsorbates after 6 recycles (Fig. 8). However, no significant changes in the adsorbent affinity toward the removal of organic pollutants (**I–IV**) from the aqueous solution were observed after several cycles, as quantitatively evidenced by the adsorbed amount per unit area of adsorbents (f_c) (see Fig. 8). In addition, the proposed monolith adsorbents retain high adsorption efficiency over commercial adsorbents, such as Amberlite IRA-904 resin, even after a number of recycles. Fig. 8 shows that the Amberlite IRA-904 adsorbent lost approximately 20% of its original efficiency after only a single regeneration/recycle, whereas the monolithic adsorbents lost 5% after six recycles. The current finding revealed that the Amberlite IRA-904 adsorbent cannot be used after four cycles. These results clearly indicate that the binding of organic adsorbates onto monolith adsorbents did not result in the degradation of the functional surface sites despite the extended recycles. Indeed, the proposed nanoadsorbent design provides easy-to-use removal assays for organic compounds and portable and reusable chemical adsorbents for a number of recycles.

Acknowledgments

Ahmed Shahat and M. Ismael thank Chemistry Department at Suez Canal University and Sohag University respectively, for granting leave of absence.

Appendix A. Supplementary data

Supplementary data associated with this article can be found, in the online version, at doi:10.1016/j.jhazmat.2011.10.088.

References

[1] S.D. Faust, O.M. Aly, Adsorption Process for Water Treatment, Butterworth Publishers, London, 1987.
[2] N.M. Ram, R.F. Christman, K.P. Cantor, Significant and Treatment of Volatile Organic Compounds in Water Supplies, Lewis Publishers, USA, 1990.
[3] D.A. Cave, P.M. Foster, Modulation of *m*-dinitrobenzene and *m*-nitrosonitrobenzene toxicity in rat sertoli-germ cell cocultures, Toxicol. Sci. 14 (1990) 199.
[4] R.E. Gosselin, R.P. Smith qnd, H.C. Hodge, Clinical Toxicology of Commercial Products, 5th edition, Williams, Wilkins, Baltimore, 1984, p. II-197.
[5] (a) A. Walcarius, L. Mercier, Mesoporous organosilica adsorbents: nanoengineered materials for removal of organic and inorganic pollutants, J. Mater. Chem. 20 (2010) 4478;
(b) K. Li, Z. Zheng, J. Feng, J. Zhang, X. Luo, G. Zhao, X. Huang, Adsorption of p-nitroaniline from aqueous solutions onto activated carbon fiber prepared from cotton stalk, J. Hazard. Mater. 166 (2009) 1180.
[6] (a) G.F. Payne, M.L. Shuler, Selective adsorption of plant products, Biotechnol. Bioeng. 31 (1988) 922;
(b) A. Uribe, P.L. Bishop, N.G. Pinto, The influence of pH and temperature changes on the adsorption behavior of organophilic clays used in the stabilization/solidification of hazardous wastes, J. Environ. Eng. Sci. 1 (2002) 123.
[7] R. Nasuto, A. Derylo, Effect of temperature on adsorption of aniline from benzene solutions on silica-gel, Pol. J. Chem. 54 (1980) 1089.
[8] E. Titus, A.K. Kalkar, V.G. Gaikar, Adsorption of anilines and cresols on NaX and different cation exchanged zeolites (equilibrium, kinetic, and IR investigations), Sep. Sci. Technol. 37 (2002) 105.
[9] M.E. Essington, Adsorption of aniline and toluidines on montmorillonite, Soil Sci. 158 (1994) 181.
[10] A.A. Gürten, S. Ucan, M.A. Özler, A. Ayar, Removal of aniline from aqueous solution by PVC-CDAE ligand-exchanger, J. Hazard. Mater. 120 (2005) 81.
[11] C. Jianguo, L. Aimin, S. Hongyan, F. Zhenghao, L. Chao, Z. Quanxing, Adsorption characteristics of aniline and 4-methylaniline onto bifunctional polymeric adsorbent modified by sulfonic groups, J. Hazard. Mater. 124 (2005) 173.
[12] (a) O. Duman, E. Ayranic, Structural and ionization effects on the adsorption behaviors of some anilinic compounds from aqueous solution onto high-area carbon-cloth, J. Hazard. Mater. 120 (2005) 173;
(b) F. Villacanas, M.F.R. Pereira, J.M. Orfao, J.L. Figueiredo, Adsorption of simple aromatic compounds on activated carbons, J. Colloids Interface Sci. 293 (2006) 128.
[13] S. Ardizzone, H. Hoiland, C. Lagioni, E. Sivieri, Pyridine and aniline adsorption from an apolar solvent: the role of the solid adsorbent, J. Electroanal. Chem. 447 (1998) 17.
[14] (a) O.G. Potter, E.F. Hilder, Porous polymer monoliths for extraction: diverse applications and platforms, J. Sep. Sci. 31 (2008) 1881;
(b) S.A. El-Safty, Functionalized hexagonal mesoporous silica monoliths with hydrophobic azo-chromophore for enhanced Co(II) ion monitoring, Adsorption 15 (2009) 227.
[15] F. Wei, J.Y. Yang, L. Gao, F.N. Gu, J.H. Zhu, Capturing nitrosamines in tobacco-extract solution by hydrophobic mesoporous silica, J. Hazard. Mater. 172 (2009) 1482.
[16] A.J. O'Connor, A. Hokura, J.M. Kisler, S. Shimazu, G.W. Stevens, Y. Komatsu, Amino acid adsorption onto mesoporous silica molecular sieves, Sep. Purif. Technol. 48 (2006) 197.
[17] (a) P.A. Mangrulkar, S.P. Kamble, J. Meshram, S.S. Rayalu, Adsorption of phenol and o-chlorophenol by mesoporous MCM-41, J. Hazard. Mater. 160 (2008) 414;
(b) S.A. El-Safty, Sorption and diffusion of phenols onto well-defined ordered nanoporous monolithic silicas, J. Colloids Interface Sci. 260 (2003) 184.

[18] S.A. El-Safty, A.A. Ismail, H. Matsunaga, H. Nanjo, F. Mizukami, Uniformly mesocaged cubic fd3m monoliths as modal carriers for optical chemosensors, J. Phys. Chem. C 112 (2008) 4825.
[19] A. Bibby, L. Mercier, Adsorption and separation of water-soluble aromatic molecules by cyclodextrin-functionalized mesoporous silica, Green Chem. 5 (2003) 15.
[20] P. Arumugam, P.T. Perumal, A new purification process for pharmaceutical and chemical industries, Org. Process Res. Dev. 9 (2005) 319.
[21] J.R. Herance, D. Das, J. Marquet, J.L. Bourdelande, H. García, Second harmonic generation of p-nitroaniline incorporated on zeolites: relative efficiencies depending on zeolite structure and film orientation, Chem. Phys. Lett. 395 (2004) 186.
[22] (a) A. Corma, Inorganic solid scids and their use in acid-catalyzed hydrocarbon reactions, Chem. Rev. 95 (1995) 559;
(b) S.A. El-Safty, Y. Kiyozumi, T. Hanaoka, F. Muzukami, Nanosized NiO particles wrapped into uniformly mesocaged silica frameworks as effective catalysts of organic amines, Appl. Catal. A: Gen. 337 (2008) 121.
[23] (a) T. Balaji, S.A. El-Safty, H. Matsunaga, T. Hanaoka, F. Mizukami, Optical sensors based on nanostructured cage materials for the detection of toxic metal ions, Angew. Chem. Int. Ed. 45 (2006) 7202;
(b) S.A. EL-Safty, A.A. Ismail, A. Shahat, Optical supermicrosensor responses for simple recognition and sensitive removal of Cu (II) ion target, Talanta 83 (2011) 1341–1351.
[24] (a) S.A. El-Safty, M. Mekawy, A. Yamaguchi, A. Shahat, K. Ogawa, N. Teramae, Organic–inorganic mesoporous silica nanostrands for ultrafine filtration of spherical nanoparticles, Chem. Commun. 46 (2010) 3917;
(b) S.A. EL-Safty, A. Shahat, W. Warkocki, M. Ohnuma, Building-block-based mosaic cage silica nanotubes for molecular transport and separation, Small 7 (2011) 62–65;
(c) S.A. EL-Safty, M.A. Shenashen, Size-selective separations of biological macromolecules on mesocylinder silica arrays, Anal. Chim. Acta 694 (2011) 151–161.
[25] (a) T. Ihor, M. Sergiy, Multiresponsive, Hierarchically structured membranes: new, challenging, biomimetic materials for biosensors, controlled release, biochemical gates, and nanoreactors, Adv. Mater. 21 (2009) 241;
(b) S.A. El-Safty, Designs for size-exclusion separation of macromolecules by densely-engineered mesofilters, Trends Anal. Chem. 30 (2011) 447;
(c) S.A. EL-Safty, A. Shahat, Md.R. Awual, M. Mekawy, Large three-dimensional mesocage pores tailoring silica nanotubes as membrane filters: nanofiltration and permeation flux of proteins, J. Mater. Chem. 21 (2011) 5593.
[26] Y. Lui, W. Zhang, T.J. Pinnavaia, Steam-stable MSU-S aluminosilicate mesostructures assembled from zeolite ZSM-5 and zeolite beta seeds, Angew. Chem. Int. Ed. 40 (2001) 1255.
[27] R. Mokaya, Ultrastable mesoporous aluminosilicates by grafting routes, Angew. Chem. Int. Ed. 38 (1999) 2930.
[28] M.C. Chao, H.P. Lin, C.Y. Mou, B.W. Cheng, C.F. Cheng, Synthesis of nano-sized mesoporous silicas with metal incorporation, Catal. Today 97 (2004) 81.
[29] M.S. Hamedy, O. Berg, J.C. Jansen, T. Maschmeyer, J.A. Moulijn, G. Mul, TiO_2 nanoparticles in mesoporous tud-1: synthesis, characterization and photocatalytic performance in propane oxidation, Chem. Eur. J. 12 (2006) 620.
[30] (a) T. Linssen, F. Mees, K. Cassiers, P. Cool, A. Whittaker, E.F. Vansant, Characterization of the acidic properties of mesoporous aluminosilicates synthesized from leached saponite with additional aluminum incorporation, J. Phys. Chem. B 107 (2003) 8599;
(b) A. Yin, X. Guo, W.L. Dai, K. Fan, Effect of Si/Al Ratio of mesoporous support on the structure evolution and catalytic performance of the Cu/Al-HMS catalyst, J. Phys. Chem. C 114 (2010) 8523.
[31] L. Gao, Z.Y. Wu, J.Y. Yang, T.T. Zhuang, Y. Wang, J.H. Zhu, Optimization of mesoporous silica through nano-casting to capture nitrosamines in environment, Microporous Mesoporous Mater. 131 (2010) 274.
[32] R. Chakravarti, H. Oveisi, P. Kalita, R.R. Pal, S.B. Halligudi, M.L. Kantam, A. Vinu, Three-dimensional mesoporous cage type aluminosilicate: an efficient catalyst for ring opening of epoxides with aromatic and aliphatic amines, Microporous Mesoporous Mater. 123 (2009) 338.
[33] J.J. Chiu, D.J. Pine, S.T. Bishop, B.F. Chmelka, Friedel–Crafts alkylation properties of aluminosilica SBA-15 meso/macroporous monoliths and mesoporous powders, J. Catal. 221 (2004) 400.
[34] (a) H. Zhu, D.J. Jones, N. Donzel, J. Zajac, M. Lindheimer, Direct synthesis of large mesopore aluminosilicates templated by lyotropic liquid crystals, Microporous Mesoporous Mater. 99 (2007) 47;
(b) S. El-Safty, A. Shahat, K. Ogawa, T. Hanaoka, Highly ordered thermally/hydrothermally stable cubic Ia3d aluminosilica monoliths with low silica in frameworks, Microporous Mesoporous Mater. 138 (2011) 51–62.
[35] (a) S.A. El-Safty, D. Prabhakaran, Y. Kiyozumi, F. Mizukami, Nanoscale membrane strips for benign sensing of Hg(II) ions: a route to commercial waste treatments, Adv. Funct. Mater. 18 (2008) 1739;
(b) S.A. El-Safty, Organic–inorganic hybrid mesoporous monoliths for selective discrimination and sensitive removal of toxic mercury ions, J. Mater. Sci. 44 (2009) 6764.
[36] (a) S.A. El-Safty, Instant synthesis of mesoporous monolithic materials with controllable geometry, dimension and stability: a review, J. Porous Mater. 18 (2011) 259;
(b) S.A. El-Safty, A review of key controls in design of copolymer-silica mesophase monoliths with large particle morphology and uniform three-dimensional pore geometry, J. Porous Mater. 15 (2008) 369.
[37] (a) F. Helferich, Ion Exchange, Mc Graw–Hill, New York, 1962;
(b) K. Inoue, K. Kawamoto, Adsorption characteristics of carbonaceous adsorbents for organic pollutants in a model incineration exhaust gas, Chemosphere 70 (2008) 349.
[38] (a) M.C. Liu, H.S. Sheu, S. Cheng, Anion-exchange induced phase transformation of mesostructured silica, J. Am. Chem. Soc. 131 (2009) 3998;
(b) Y. Zhang, P.S. Cremer, Interactions between macromolecules and ions: the Hofmeister series, Curr. Opin. Chem. Biol. 10 (2006) 658.
[39] (a) P.I. Ravikovitch, A.V. Neimark, Density functional theory of adsorption in spherical cavities and pore size characterization of templated nanoporous silicas with cubic and three-dimensional hexagonal structures, Langmuir 18 (2002) 1550;
(b) K. Michal, A. Valentyn, R.M. Jivaldo, P.M. Lucildes, J. Mietek, Determination and tailoring the pore entrance size in ordered silicas with cage-like mesoporous structures, J. Am. Chem. Soc. 124 (2002) 768;
(c) S.A. El-Safty, T. Hanaoka, F. Mizukami, Design of highly stable, ordered cage mesostructured monoliths with controllable pore geometries and sizes, Chem. Mater. 17 (2005) 3137;
(d) J.M.R. Gallo, C. Bisio, G. Gatti, L. Marchese, H.O. Pastore, Physicochemical characterization and surface acid properties of mesoporous [Al]-SBA-15 obtained by direct synthesis, Langmuir 26 (2010) 5791.
[40] M.N. Timofeeva, V.N. Panchenko, A. Gil, Y.A. Chesalov, T.P. Sorokina, V.A. Likholobov, Synthesis of propylene glycol methyl ether from methanol and propylene oxide over alumina-pillared clays, Appl. Catal. B Environ. 102 (2011) 433.
[41] C.L. Cavalcante Jr., D.M. Ruthven, Adsorption of branched and cyclic paraffins in silicalite. 2. kinetics, Ind. Eng. Chem. Res. 34 (1995) 185.
[42] S.A. El-Safty, A.A. Ismail, H. Matsunaga, H. Nanjo, F. Mizukami, Optical nanosensor design with uniform pore geometry and large particle morphology, Chem. Eur. J. 13 (2007) 9245.
[43] A.K. Chandra, T. Uchimaru, The O–H bond dissociation energy of substituted phenol and proton affinities of substituted phenoxide ions: a DFT study, Int. J. Mol. Sci. 3 (2002) 407.
[44] D. Vasudevan, A.T. Stone, Adsorption of catechols, 2-aminophenols, and 1,2-phenylenediamines at the metal (Hydr)oxide/water interface: effect of ring substituents on the adsorption onto TiO_2, Environ. Sci. Technol. 30 (1996) 1604.